ELSEVIER

Applied Surface Science 197–198 (2002) 791–795

applied surface science

www.elsevier.com/locate/apsusc

Influence of the irradiation wavelength on the ablation process of designed polymers

M. Hauer[a], T. Dickinson[b], S. Langford[b], T. Lippert[a,*], A. Wokaun[a]

[a]*Paul Scherrer Institute, 5232 Villigen PSI, Switzerland*
[b]*Washington State University, Pullman, Washington, DC 99164-2814, USA*

Abstract

A photolabile triazene polymer was irradiated with a KrF (248 nm) and a XeCl (308 nm) excimer laser. The resulting ablation fragments were analyzed using time of flight mass spectroscopy (TOF-MS). The peak intensities of the main ablation fragments reveal a pronounced influence of the irradiation wavelength and fluence. After 248 nm irradiation the peak intensities of all polymer fragments reach maxima at high fluences whereas after 308 nm irradiation only the 168 amu peak intensity reaches a maximum. All other analyzed fragments (28, 35 and 76/77 amu) do not reveal a maximum. The time of arrival curves of the decomposition products at both irradiation wavelengths are composed of three distinctive components. Two quite sharp peaks are fitted by a Gaussian distribution, whereas a third broad peak is described by a decaying Maxwell–Boltzmann distribution. The first fast peak is attributed to the fragments produced during the laser pulse. The second peak was detected around 100 μs after the laser pulse. The peak is very sensitive to the alignment of the setup, but very insensitive to changes in the electrical fields, and was still pronounced after grounding the ionizer. Therefore the peak was assigned to excited neutral nitrogen molecules (metastable N_2).

Keywords: Laser ablation; Time of flight mass spectroscopy; Metastable nitrogen

1. Introduction

In the last two decades the ablation of polymers has been studied in detail. Despite the use of variety of characterization techniques, the ablation mechanism is still controversial. It has been repeatedly emphasized [1,2] that it is important to analyze the product distribution and the kinetic energy in order to understand the ablation process. Many different polymers were studied under different experimental conditions using time of flight mass spectroscopy (TOF-MS). The fragments which are released during the ablation process range from small degradation products [3,4], to monomers [5,6], to carbon clusters [7], and polymer fragments with masses up to 2500 amu [8,9]. The kinetic energies of many fragments follow a Maxwell–Boltzmann distribution with temperatures consistent with a photothermal decomposition process [10–12], whereas for other polymer fragments much higher temperatures were derived [13,14].

A photolabile triazene polymer with excellent laser ablation properties (sharp ablation edges, no debris, low threshold fluence and high etch rates at low fluences [15]) has been studied previously by TOF-MS [16,17]. The time of arrival curves could not be explained by simple Maxwell–Boltzmann energy distributions. The polymer was irradiated with a KrF excimer laser (248 nm) and only the 28 and 76 amu

* Corresponding author. Tel.: +41-56-310-4076; fax: +41-56-310-2485.
E-mail address: thomas.lippert@psi.ch (T. Lippert).

0169-4332/02/$ – see front matter
PII: S0169-4332(02)00416-6

fragments were analyzed. In this work we study the differences in the TOF-MS measurements after irradiation with a KrF (248 nm) and a XeCl excimer laser (308 nm). This is especially interesting as the absorption band of the triazeno group is located around 330 nm. Additional masses, i.e. 35 amu (chlorine from the solvent), and 168 amu (a primary fragment from the polymer) were included in the analysis.

2. Experimental

The synthesis of the triazene polymer is described in detail elsewhere [18]. The repetition unit and the suggested exothermic decomposition pathway of the polymer are described in Fig. 1. The UV–Vis absorption spectrum of the polymer shows two absorption maxima. The absorption maximum around 330 nm is mainly due to the triazeno group, whereas the absorption maximum at 200 nm can be assigned to the aromatic system [19]. The absorption minimum between these bands is centered near 250 nm. The polymer samples were prepared by solvent casting from a chlorobenzene solution (10 wt.%) and kept in vacuum overnight. The polymer films were irradiated with excimer lasers (Lambda Physik EMG 203 MSC (XeCl) and Lambda Physik LPX 205 I (KrF)). The emissions were detected with a UTI 100C quadrupole mass spectrometer with the ionizer mounted 10.5 cm from the sample. Time of arrival signals for the different species were recorded with an EG&G PARC 914P multichannel scaler. The kinetic energies of the fragments were analyzed with curve fitting techniques. The employed model was described in detail elsewhere [16,17]. Briefly, the emission of the slow component is described by a thermally activated process, while the fast components were fitted to Gaussian energy distributions appropriate for either ground state or excited neutrals.

3. Results and discussion

3.1. Fluence dependence of the fragment intensities

The suggested decomposition scheme (Fig. 1) of the polymer shows one major fragment (N_2, 28 amu) from the decomposition of the triazeno group. Other primary fragments are 168 amu (biphenylether) and 142 amu from the aliphatic diamine group. No attempt was made to resolve fragments at 77 and 76 amu; these may correspond to either products of direct ablation products or to products of secondary decomposition of the biphenylether moiety or residual solvent (chlorobenzene). The 35 amu signal can be uniquely assigned to chlorine from residual solvent.

The peak intensities of the different fragments after irradiation with a XeCl excimer laser at different fluences is shown in Fig. 2. The fluence dependence of the N_2 fragment exhibits a linear behavior at low fluences (not shown) corresponding to photodecomposition. At fluences above 40 mJ cm^{-2}, a fast (non-linear) increase is observed. This non-linear behavior is probably due to the onset of ablation, which is defined as the start of material removal. Ablation is normally associated with enhanced fragmentation and

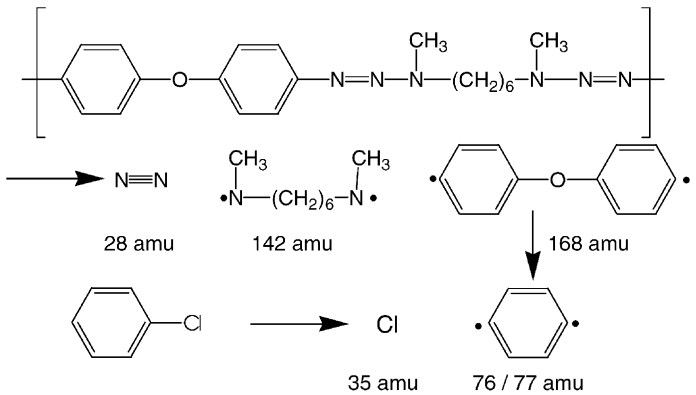

Fig. 1. Chemical structure and suggested decomposition pathway of the triazene polymer.

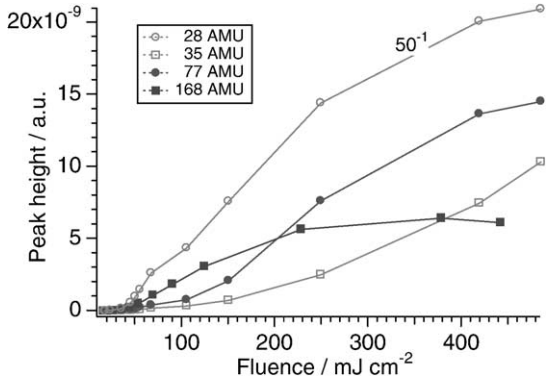

Fig. 2. Fluence dependence of the peak intensities of the fragments after irradiation with a XeCl excimer laser.

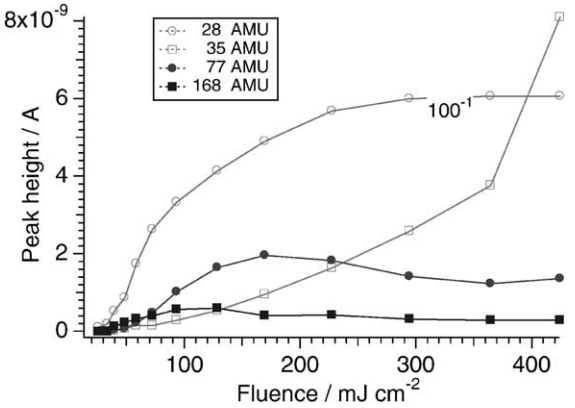

Fig. 3. Fluence dependence of the peak intensities of the fragments after irradiation with a KrF excimer laser.

a higher quantum yield then in the photodecomposition. These changes in the increase of the peak intensities occur in the range (25–50 mJ cm^{-2}), where the ablation threshold was detected by other methods [19,20]. The 35 amu signal exhibits a strongly nonlinear behavior over the whole fluence range. This can be explained by two different factors. At low fluences, the signal may be weak because of a dense surface layer with less solvent, as suggested in previous work with PMMA [14]. This layer is ablated at higher fluences, which results in the decomposition of polymer with a higher solvent concentration. Another factor could be higher surface temperatures at higher fluences, which may thermally decompose chlorobenzene. The 76/77 amu fragment is due to the decomposition of the solvent and secondary fragmentation of the biphenylether group (168 amu). At lower fluences, the 76/77 amu appears similar in shape to the 35 amu signal, while at higher fluences, it correlates better with the 168 amu fragment. At low fluences the 168 amu signals increase is similar to the 28 amu signal, but it plateaus at higher fluences, probably due to secondary fragmentation.

The fluence dependence of the peak intensities under 248 nm irradiation is significantly different, as shown in Fig. 3. At 28 amu, no linear increase at low fluences is detected, while at high fluences the signal plateaus. This effect is probably due to absorption of incoming photons by aromatic fragments, which are released during ablation. The 35 amu curve increases slowly at the beginning and much faster at high fluences, similar to its behavior at 308 nm. The 76/77 amu signal increases slowly at low fluences, reaches a peak at about 170 mJ cm^{-2}, then decreases slightly. Significantly, the 168 amu signal displays similar behavior, but peaks earlier, at about 130 mJ cm^{-2}. We attribute part of the increase in the 76/77 amu fragment between 130 and 170 mJ cm^{-2} to fragmentation of the 168 amu (biphenylether) fragment. At still higher fluences, photodecomposition of phenyl moieties would decrease the signals at both 76/77 and 168 amu.

3.2. Time of arrival curves

Fig. 4 shows the TOF curves of the N_2 fragment for both irradiation wavelengths. Both curves show three distinct components. A fast component with a peak TOF signal around 40 μs is detected after irradiation with both laser wavelengths. This peak was modeled by a Gaussian energy distribution and can be attributed to the fast fragments described in the previous papers [16,17]. Around 70 μs (308 nm) and 95 μs (248 nm) after the laser pulse, respectively, a second peak appears. This peak was not detected in the previous measurements with this polymer.

This peak is very sensitive to the alignment of the sample with respect to the quadrupole. The peak becomes prominent only in the presence of a line-of-sight path from the laser spot, through two internal apertures, and terminated on the quadrupole particle detector. Great care was taken in the present measurements to insure accurate alignment. Additional analysis

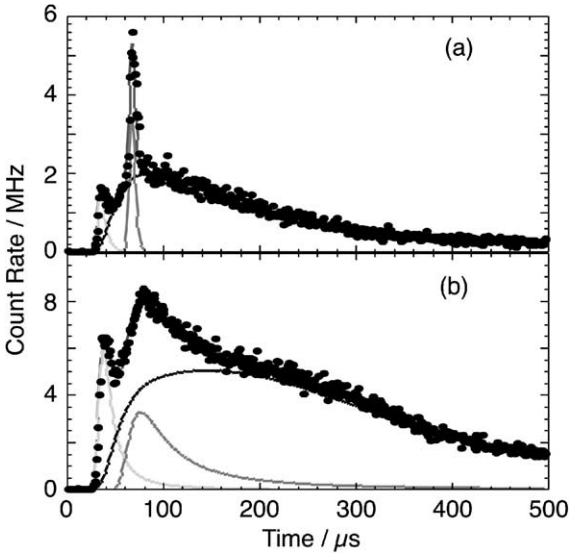

Fig. 4. Time of arrival curves of the 28 amu fragment after irradiation with a fluence of 260 mJ cm^{-2} with (a) XeCl, and (b) KrF excimer laser. The fits to the components are included in the figure.

of this peak revealed that the mass filter had little effect on the signal intensity. Similarly, strong electric fields applied to the ionizer optics had little effect. Therefore, we attribute this peak to uncharged neutral fragments. In this work, detection of neutral particles requires internal energies of at least 4–5 eV. A most likely candidate for such fragments is the first excited electronic state of the N_2 molecule ($A^3\Sigma_u^+$). The third component of the TOF curves consists of a broad tail, which extends hundreds of microseconds after the laser pulse. The tail was fitted by a Maxwell–Boltzmann distribution with decaying temperature as described previously [16,17].

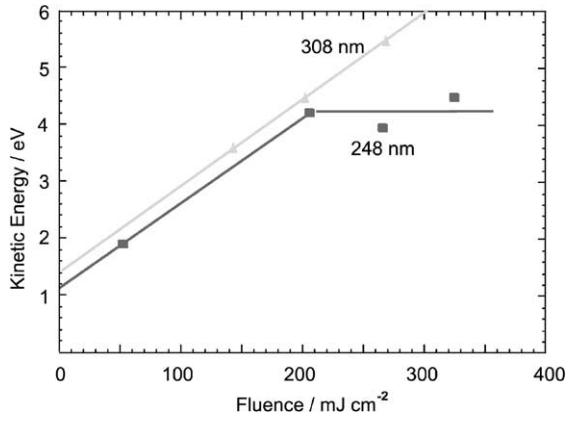

Fig. 5. Fluence dependence of the kinetic energies of the fast peak in the time of arrival curves.

Fig. 5 shows the fluence dependence of the kinetic energy of the fast peak. A linear increase is observed for low fluences at 248 nm, followed by a plateau at higher fluences (>250 mJ cm^{-2}). A similar linear increase of the kinetic energy with fluence is obtained at 308 nm; at the highest fluences, the kinetic energies of the fast peak exceed those observed at 248 nm. At both wavelengths, the observed kinetic energies are well above values expected from thermal emission processes.

4. Conclusions

The peak intensities of the mass selected TOF signals are profoundly influenced by irradiation wavelength and fluence. After 248 nm irradiation an enhanced fragmentation of the heavier fragments is observed. This is probably due to absorption of the incoming laser beam by absorbing fragments, e.g. the phenyl and the biphenylether fragments. This shielding effect limits the number of photons reaching the surface, which is supported by the lower etch rates at 248 nm irradiation at higher fluences [21]. The time of arrival curves show three distinctive components: two fast peaks were observed, which were fitted to Gaussian energy distributions, along with a third, slow peak, which was fitted by a decaying Maxwell–Boltzmann distribution. The arrival time of the fastest peak corresponds to kinetic energies of 2–5 eV, which are well above values expected for thermal processes. A second peak was attributed to metastable N_2, while the third peak may be described by a thermal process.

Acknowledgements

This work was supported by the Swiss National Science Foundation, a NATO Grant for International Collaboration (CRG 973063), and the United States Department of Energy under Contracts DE-FG06-92ER14252 and DE-FG03-98ER14864.

References

[1] R. Srinivasan, B. Braren, Chem. Rev. 89 (1989) 1303.
[2] R. Srinivasan, Appl. Phys. A 56 (1993) 417.
[3] R.C. Estler, N.S. Nogar, Appl. Phys. Lett. 49 (1986) 1175.
[4] D.J. Krajnovich, J. Phys. Chem. A 101 (1996) 2033.
[5] J.T. Dickinson, J.-J. Shin, W. Jiang, M.G. Norton, J. Appl. Phys. 74 (1993) 4729.
[6] G.B. Blanchet, J.C.R. Fincher, Appl. Phys. Lett. 68 (1996) 929.
[7] S.G. Hansen, J. Appl. Phys. 66 (1989) 1411.
[8] R. Srinivasan, B. Braren, D.E. Seeger, R.W. Dreyfus, Macromolecules 19 (1986) 916.
[9] R. Larciprete, M. Stuke, Appl. Phys. B 42 (1987) 181.
[10] M. Tsunekawa, S. Nishio, H. Sato, J. Appl. Phys. B 76 (1994) 5598.
[11] M. Tsunekawa, S. Nishio, H. Sato, Jpn. J. Appl. Phys. 34 (1995) 218.
[12] B. Danielzik, N. Fabricius, M. Röwekamp, D.V.D. Linde, Appl. Phys. Lett. 48 (1986) 212.
[13] D. Feldmann, J. Kutzner, J. Laukemper, S. MacRobert, K.H. Welge, Appl. Phys. B 44 (1987) 81.
[14] T. Lippert, R.L. Webb, S.C. Langford, J.T. Dickinson, J. Appl. Phys. 85 (1999) 1838.
[15] T. Lippert, J. Stebani, J. Ihlemann, O. Nyken, A. Wokaun, J. Phys. Chem. 97 (1993) 12296.
[16] T. Lippert, A. Wokaun, S.C. Langford, J.T. Dickinson, Appl. Phys. A 69 (1999) 655.
[17] T. Lippert, S.C. Langford, A. Wokaun, G. Savas, J.T. Dickinson, Appl. Phys. A 89 (1999) 7116.
[18] J. Stebani, O. Nyken, T. Lippert, A. Wokaun, Makromol. Chem. Rapid Commun. 206 (1993) 2943.
[19] T. Lippert, L.S. Bennett, T. Nakamura, H. Niino, A. Ouchi, A. Yabe, Appl. Phys. A 63 (1996) 257.
[20] J. Wei, N. Hoogen, T. Lippert, O. Nuyken, A. Wokaun, J. Phys. Chem. B 105 (2001) 1267.
[21] T. Lippert, A. Wokaun, J. Stebani, O. Nyken, J. Ihlemann, Angew. Makromol. Chem. 206 (1993) 97.